GRB 161219B/SN 2016jca: a powerful stellar collapse.

C.Ashall[1], E.Pian[2,3], P.A. Mazzali[1,4], E.Palazzi[2], S.J.Prentice[1], S.Kobayashi[1], A.Levan[5], D.Perley[1], F. Bufano[6], A.V.Filippenko[7], J.P.U.Fynbo[8], A. Melandri[9], S.Oates[5], A.Rossi[2], J.Selsing[8], W.Zheng[7], A.J.Castro Tirado[10], G.Chincarini[9], P.D'Avanzo[9], M. De Pasquale[11], S.Emery[11], A.S. Fruchter[12], K.Hurley[13], D.Malesani[8] P.Moller[14], K.Nomoto[15], M.Tanaka[16], N.Tanvir[17], A.F.Valeev[18]

Authors affiliations can be found at the end of the text.

arXiv:1702.04339v2 [astro-ph.HE] 15 Feb 2017

Long duration gamma-ray bursts (GRBs) mark the birth of a compact object, a neutron star or black hole. At low-redshift ($z < 0.2$) these events are extremely rare and most are poorly known. Four nearby GRBs have been associated with Type Ic supernovae (SNe Ic), [1, 2, 3, 4, 5, 6, 7]. GRB/SNe lack hydrogen and helium, and are classified as SNe Ic, but have extremely broad features, which indicate the presence of material at very high velocities ($> 0.3c$)[8]. They have a kinetic energy (E_k) of $\gtrsim 10^{52}$ erg, and are thought to be the explosion of bare carbon-oxygen cores of stars with initial mass 35-50 $M_\odot$[9]. Here we report observations of the nearby GRB 161219B ($z = 0.1475$, [10]) and the associated SN2016jca. We obtained a high-cadence time-series of spectra and photometry starting 2 days after explosion. The GRB afterglow had a late achromatic break 12 days after outburst which indicates that the relativistic material was ejected in an outflow with a large opening angle. We first identified the SN 5 days after the GRB [11]. Such an early detection gives us the opportunity to explore the outermost layers of the ejecta. We find the outer most ejecta are dominated by heavy elements, while lighter elements are present in high abundance at low velocities. Geometrically this suggests that we are viewing a high velocity nuclearly processed outflow down its axis. This and the wide opening angle suggests a highly magnetized millisecond pulsar may power the explosion.

GRB 161219B exploded on 19-12-2016. Our HST image (Figure 1) shows that SN 2016jca is located in an edge-on spiral galaxy; an analysis of the host galaxy emission lines at the location of the transient, based on a VLT X-Shooter spectrum, indicates a metallicity range $0.3 < Z/Z_\odot < 0.55$. This is characteristic of other low-redshift gamma-ray burst host galaxies [20, 21, 22, 23].Ten spectra of the optical transient were obtained between 1.99 and 32.65 days (rest frame) after explosion. The first spectra are dominated by the afterglow, and at $t = 5.52$ d the SN is clearly visible. The spectral features are typical of previously observed

Supplementary material can be found at `https://www.astro.ljmu.ac.uk/~astcasha/SN2016jcasupplemantary.pdf`

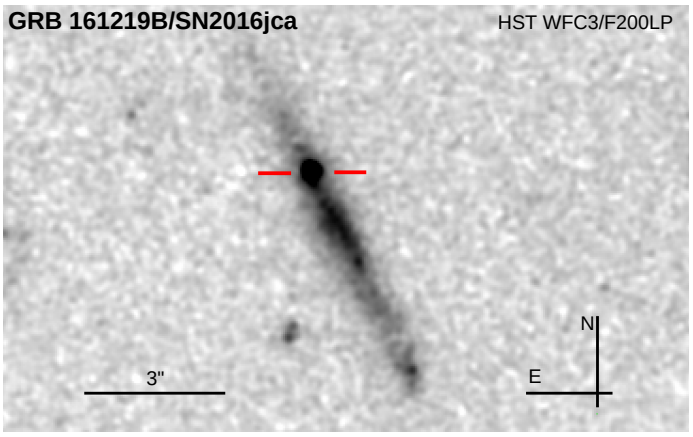

Figure 1: *HST* WFC/UVIS and F200LP open filter (2000-10000 Å) image of the field of GRB 161219B. The optical transient is located in the north east corner of the elongated spiral galaxy.

GRB/SNe [1] such as SN 1998bw, which warrants a classification as "Ic-3" [12]. SN ejecta can be assumed to be in homologous expansion ($r = vt_{\rm exp}$, where r is the distance from the centre of the explosion, v the velocity, and $t_{\rm exp}$ the time from explosion). As time passes, progressively deeper layers of the ejecta are exposed. The early-time spectra of SN 2016jca are critical to test current GRB-SN models and determine the physics of the outermost layers in the explosion.

Before the spectra and light curve of the SN can be examined the GRB afterglow must be understood and removed, particularly at early epochs. The initial (< 2 d) decline of the optical and X-ray light curves can be attributed to a monotonically decreasing afterglow formed via synchrotron radiation in a relativistic blast wave, while the optical flattening associated with SN 2016jca is detected starting 2–3 days after explosion. The optical-to-X-ray spectral energy distribution of the afterglow before day 2 suggests that at these early epochs the synchrotron cooling frequency is located between the optical and X-rays, and that the relativistic particles distribution in the jet has a flat spectrum (E^{-p}, with $p < 2$). Combined with the observed afterglow temporal decay, this is consistent with the standard fireball formalism, if the blast wave is re-energized at < 0.1 day after explosion [44, 45]. If the steepening of the X-ray light curve with respect to a single power-law at about 12 days is related to the physical edge of a homogeneous jet, a full opening angle of about 40 degrees is derived. Correcting the GRB isotropic energy (1.6×10^{50} erg, [13]) for the solid angle subtended by the jet aperture, an energy of $\sim 10^{49}$ erg is obtained.

After subtracting the afterglow model from the observed optical light curves we constructed the SN bolometric light curve (Figure 2). The SN reaches bolo-

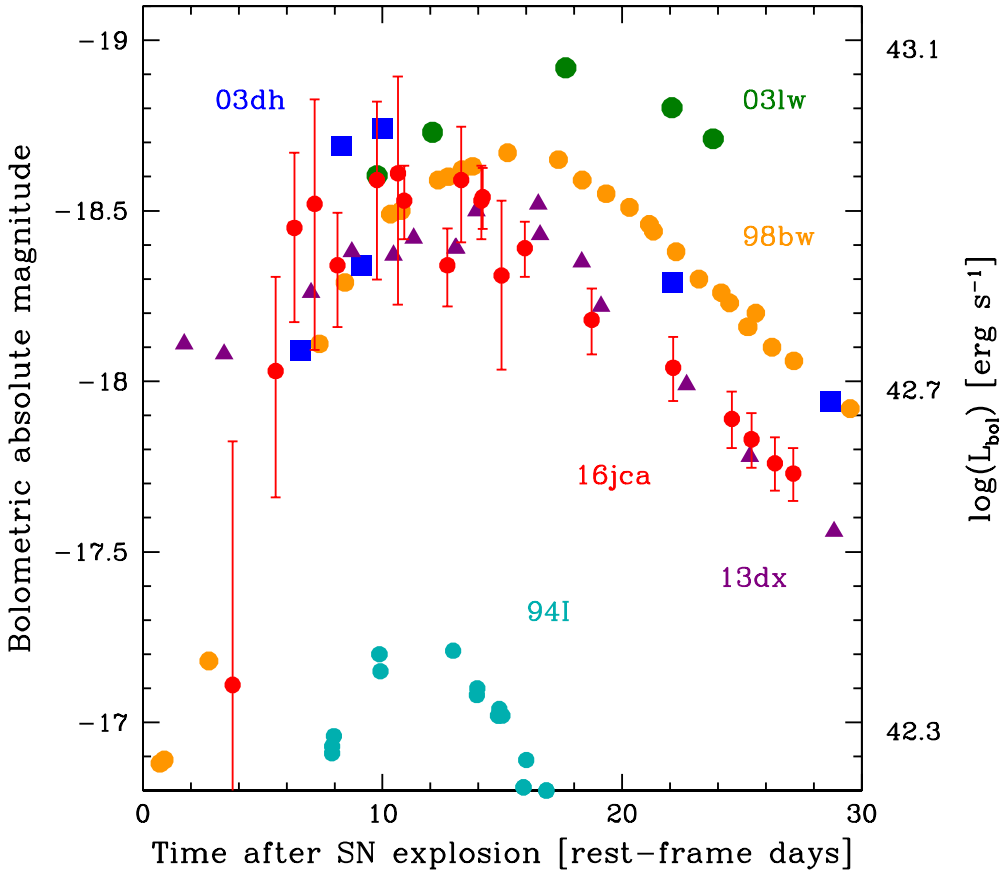

Figure 2: Pseudo-bolometric light curve (3000–10,000 Å) of SN 2016jca after the subtraction of the host galaxy and afterglow components, compared with bolometric light curves of previous GRB-SNe 1998bw, 2003dh, 2003lw, 2013dx [1, 14, 5, 6], and "normal" Ic SN1994I (not associated with a GRB) [15, 16]. To avoid confusion, the error bars are only shown for 2016jca. The errors on 1998bw are smaller than the markers, and the errors on 2003dh, 2003lw and 2013dx are comparable with those of 2016jca. The first points, like in SN2003dh and 2013dx, are heavily contaminated by the afterglow.

metric peak $\sim$12 d after the GRB at -18.6 mag. This requires roughly 0.4 $M_\odot$ of radioactive ^{56}Ni, whose decay to ^{56}Co and ^{56}Fe powers the optical display. These values are similar to the average rise-time, peak bolometric magnitude and ^{56}Ni of well-observed GRB-SNe ($\sim 14 \pm 2$ d, $\sim -18.7 \pm 0.2$ mag $\sim 0.4 \pm 0.1$ $M_\odot$). The rise-time is significantly shorter (3 days) than that of SN 1998bw, the prototypical GRB-SN. This may imply that the ejecta of SN 2016jca are somewhat less massive than those of SN 1998bw, as mass is the main driver of light curve width, or that the viewing angle to the SN symmetry axis is different, or both. If the SN is viewed down the axis of the GRB jet, it is expected that there will be ^{56}Ni further out in the ejecta facing the observer [46]. Hence, SN 2016jca peaks more rapidly.

SN 2016jca and SN 1998bw are spectroscopically similar, but not identical. Both have a strong high-velocity Ca II near-infrared (NIR) triplet, indicating a large opacity at $v > 0.2c$, and show a weak Si II absorption feature at 5800 Å. However, SN 2016jca shows a stronger blend of metal lines (Fe II, Co II, and Ti II) in the wavelength range 4000–5000 Å, and a much weaker oxygen absorption at 6800 Å, indicating that we are observing a region where nuclear burning was more efficient and reached higher up the α-chain.

To compare quantitatively SN 2016jca to other GRB-SNe, we turn to spectral models. We use a 1D Monte Carlo SN spectrum synthesis code to produce synthetic SN spectra at nine epochs (Figure 4). The code follows the propagation of photon packets, which are emitted from a blackbody photosphere, through the SN ejecta [18]. The code requires a given density profile and allows the user to vary abundances, time from explosion, photospheric velocity, and bolometric luminosity to produce optimally fitting synthetic spectra. Producing a time series of synthetic spectra, which match observations, we can explore the physical properties of different layers in ejecta. This allows us to determine an explosion scenario for the SN.

We initially produced synthetic models using the density profile of GRB030329-SN 2003dh [8], but these models could not produce the high velocity (0.14c) Si II feature seen at 5.52 d. Therefore, a flattening of the density profile in the outermost layers was required to cause increased absorption, line broadening and blending. The first model at $t = 3.73$ d probes the outermost layers; it has $v_{\rm ph} = 44,000$km s^{-1} ($\sim 0.15c$). The model produces a good fit indicating that the density structure of the outer layers of the explosion is approximately correct. With this structure all later models are well fit, see Figure 5. SN 2016jca has the highest velocity of any GRB-SN. The same absorption features can be seen throughout all of the presented models. A high abundance of metals significantly above the photosphere is required to match the observations. All early models have higher Cr, Fe, Co, and Ni abundances than SN 1998bw. The Ni abundance is larger at higher velocities. This is very unlikely to be the property of a spherically symmetric explosion, see Figure 3. It could however be the result

of SN 2016jca being viewed closer to the jet axis. A larger covering fraction of processed beamed outflow material at high velocities can be expected given the epoch of the first spectrum and the large opening angle. This is indirect proof that the SN is intrinsically highly aspherical, especially in element distribution [17]. This agrees with nebular models of SN 1998bw, where it was found that Fe was expanding more rapidly than oxygen [19], suggesting that the explosion was aspherical.

The density profile we used for SN 2016jca has an ejecta mass of 8 $M_\odot$ and an isotropic $E_k = 5.4 \times 10^{52}$ erg. This is consistent with all other GRB-SN. The actual E_k of all GRB-SN is presumably smaller because the explosion is aspherical [46]. As our data probe the previously unexplored outermost layers of a GRB-SN, we have been able to determine that there is a significant amount of Ni-rich material moving at a velocity in excess of $\sim 0.15c$. Our models have 0.9 $M_\odot$ above $0.1c$ and 0.06 $M_\odot$ above $0.2c$. The presence of significant mass at such high velocities may represent a connection with the relativistic outflow. However, despite the high abundance we find only $\sim$0.1$M_\odot$of ^{56}Ni above 16000km s^{-1}. Compared to what is required to drive the light curve this means that most of the ^{56}Ni is at low velocities, as was the case for SN 1998bw [19].

Well studied GRB/SNe have all remarkably similar properties. The similarity in mass and E_k of all GRB-SN points to similar progenitors and explosion mechanism [9]. The progenitors are thought to be low-metallicity (i.e. moderately sub-solar) Wolf-Rayet stars with initial masses of the order of $\sim$35–50 $M_\odot$. A neutron star appears as a more suitable remnant candidate for GRB-SN explosion than a black hole in view of the relative constancy of the physical parameters of these objects. The rotational energy of a millisecond pulsar (a few 10^{52} erg) is extremely similar to the kinetic energy of all GRB-SNe [24].

A possible scenario is that the collapse of a compact carbon-oxygen core of a Wolf-Rayet (-like) star produces a short-lived, highly magnetized neutron star (magnetar) and SN. The magnetar spins down and could inject a burst of energy into the SN ejecta, producing the large E_k of GRB-SNe, and possibly contributing to the nucleosynthesis [26]. The magnetar may then accrete material from the SN ejecta and collapse into a black hole [28], or simply slow down and collapse because it was overly massive and sustained by rotation, in either case a GRB is produced. The energy output of the GRB, corrected for jet collimation angle, is of the same order as the other low-redshift GRBs with accompanying SN, whose energies top at $\sim 3 \times 10^{50}$ erg [24]. This is consistent with the energy dissipated by a highly magnetized millisecond pulsar and the possible presence of a refreshed shock in the afterglow of GRB161219B provides further evidence for a pulsar engine [25, 26, 27]. Regardless of the nature of the central engine, the extremely small ratio (less than 0.1%) between the energy promptly emitted by GRB161219B and the kinetic energy of SN 2016jca underlines the fact that the

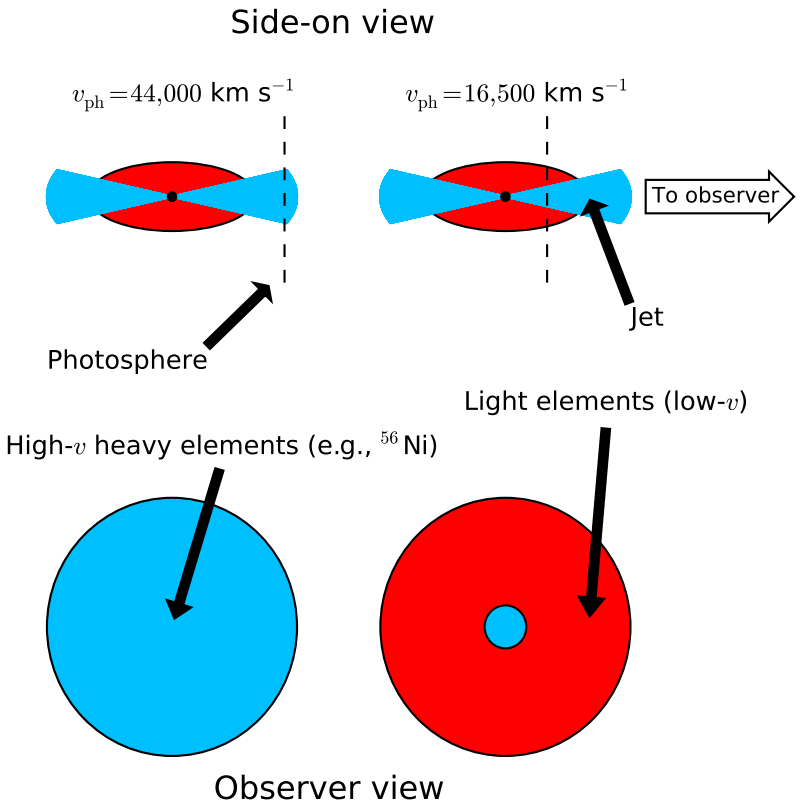

Figure 3: A demonstration of the ejecta velocity distribution in an aspherical explosion with jet component and the dependence on photospheric velocity $v_{\rm ph}$ for spectral line velocities. All material to the left of the photosphere is optically thick to the observer, while material to the right is optically thin, this is where line formation formation occurs. (Left) At $v_{\rm ph} = 44,000$ km s^{-1} the photosphere forms inside the jet and so only high-velocity material contributes to spectral line formation. (Right) At a lower $v_{\rm ph}$ the photosphere forms across both the high- and low-velocity material providing a range of line velocities in the spectra. The figure is for illustration purposes only.

main event is the SN.

Methods

The data, methods, and modelling code are described here. We provide details on the data reduction, and present the different data used. We demonstrate how the afterglow subtraction was performed. Finally, we explain how the synthetic spectra are produced and how the modelling code works.

Optical photometric and spectroscopic observations of GRB 161219B/SN 2016jca commenced on December 22.08 (UT), or 1.99 days after explosion in the rest frame. Spectra and *BVRI* photometry were obtained using FORS2 on the VLT. The transient was also observed in *BVgri* using IO:O on the 2 m Liverpool Telescope (LT) and in BVRI using the DOLORES camera on the Italian 3.6 m Telescopio Nazionale Galileo (TNG) at Observatorio del Roque de Los Muchachos, Spain. Photometry was also obtained with the LRIS instrument at the Keck observatory.

Photometric instrumental magnitudes were calculated using aperture photometry through a custom PYTHON pipeline utilising the IRAF DAOPHOT package as part of UREKA. At each epoch, a variable aperture was fit over each source in the field and the resulting instrumental magnitudes calibrated to local standard stars. FORS2 photometry was calibrated against secondary photometric standards in the field of view of the target (see Supplementary Table 1). The local standards have been chosen among isolated stars in regions of constant background, and far away from bright and saturated objects. Their point-spread function magnitudes were obtained with the same photometric zero point used to calibrate the magnitudes of stars in the Landolt fields SA95 and SA98 observed (respectively) before and after SN 2016jca on the nights of 22 and 29 December. The LT photometry was calibrated to stars from the American Association of Variable Star Observers Photometric All-Sky Survey (APASS) Data Release 9. The TNG data reduction, including de-biasing and flat-fielding, was carried out following standard procedures: the cross-calibrated magnitudes were obtained using aperture photometry with respect to the secondary standard stars reported in Supplementary Table 1.

Optical low-resolution spectra were acquired at the VLT with the FORS2 spectrograph and varying setups (see log of observations in Supplementary Table 2). During some of the epochs when the 300V grism was used, we also applied an order-separating filter, owing to severe contamination long-ward of 6000 Å by second-order light.

The 2D spectral images were flat-fielded and debiased, and the 1D spectra were optimally extracted [31] and reduced following standard procedures within IRAF. They were then linearised and calibrated against catalogued spectrophoto-

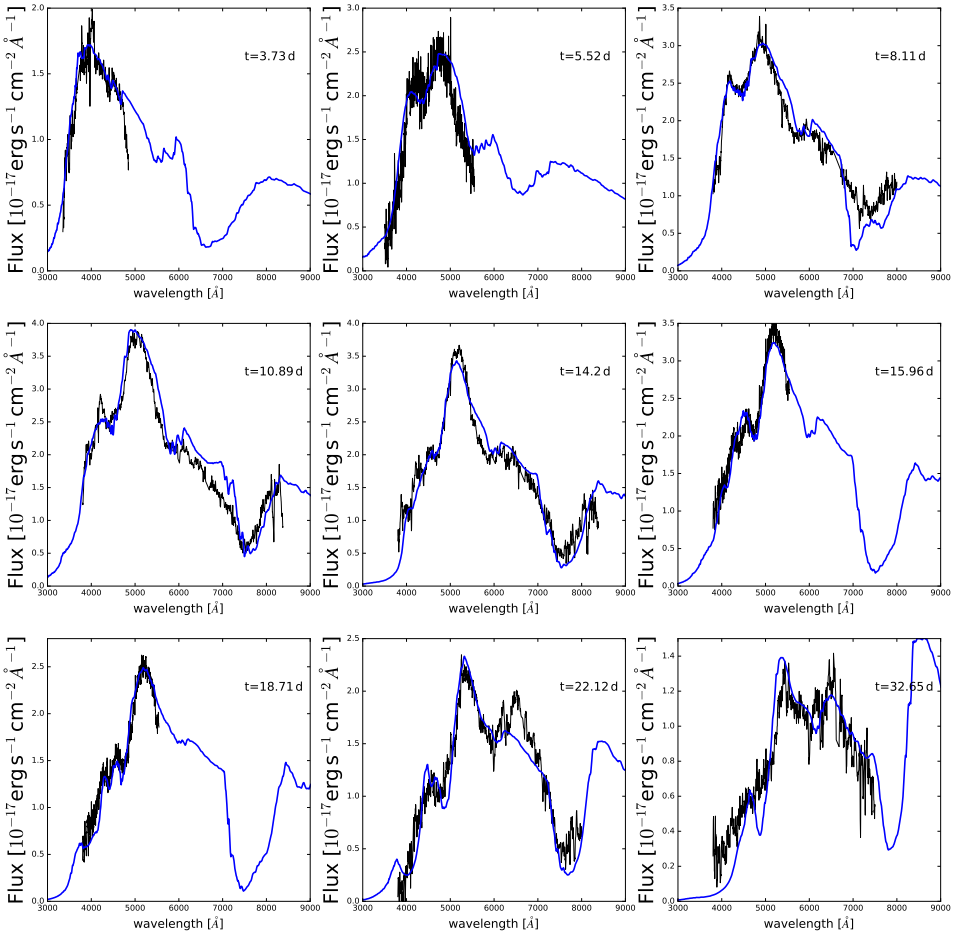

Figure 4: VLT FORS2 spectra of SN 2016jca in rest-frame (black) and models at nine epochs. The spectra are corrected for Galactic extinction ($E_{B-V} = 0.028$), and smoothed with a 15-Å boxcar. The host galaxy and afterglow components were subtracted.

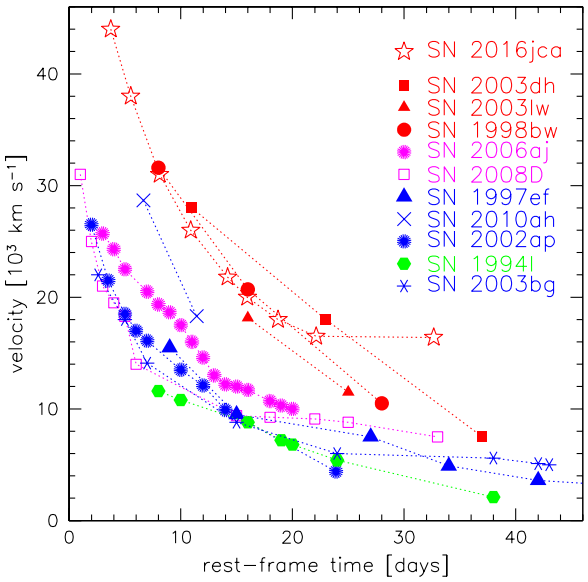

Figure 5: Photospheric velocity, as determined from spectral models, as a function of time from explosion for 11 modelled SNe. The red points are GRB/SNe, the pink points are SNe associated with X-ray flashes. The blue symbols are high KE SNe with no detected accompanying high energy event. SN 1994I is a normal SN Ic. The velocity of the photosphere drops from rapidly over the first 18.39 days. The velocity is at the high end of the distribution for GRB-SNe (see Figure 5). SN 2016jca was observed as early as SN 2002ap [3]; however, it shows much higher velocities. At later times, SN 2016jca evolves like other GRB-SNe but with a higher velocity, which highlights the similarity among these events as well as their exceptionally high energies.

metric standards, and corrected for atmospheric extinction. The flux calibration was refined by comparison with the simultaneous photometry. Telluric lines and weak emission lines from the host galaxy were removed.

The host galaxy of the GRB-SN is clearly detected and resolved in both the VLT images and a *Hubble Space Telescope (HST)* image taken with WFC3/UVIS and the open LP filter (about 2000–10,000 Å); see Figure 1. We have located, on archival PanStarrs images of the host, the precise position of the GRB-SN using the *HST* LP image and have measured the flux of the host within a circle of $1''$ radius. The $griz$ magnitudes are $g = 23.0 \pm 0.1$, $r = 22.6 \pm 0.1$, $i = 22.4 \pm 0.1$, and $z = 22.5 \pm 0.1$. The resulting colours are typical of a modestly absorbed star-forming galaxy [32]. We have converted these magnitudes to the Bessel $BVRI$ system for subtraction from the optical counterpart; see below.

We applied a Galactic extinction correction using $E(B-V) = 0.028$ mag [33] and the extinction curve of [34], and a K-correction that we evaluated with our own spectra, to our $BVRI$ light curves. These are reported in Supplementary Figure 2 in the rest frame. While the initial decline can be attributed to a monotonically decreasing afterglow formed in a blast wave, starting around day 2–3 all light curves show a rebrightening that we interpret as supernova emission, as clearly confirmed by the spectra that exhibit the typical stripped-envelope supernova signature. We have decomposed the light curves into an afterglow component, a supernova similar to SN 1998bw [1], and a host galaxy estimated as stated above.

The X-ray afterglow of GRB 161219B was observed by the *Swift*/XRT (0.3–10 keV) and by the *Swift*/UVOT with its 6 optical and UV filters. The X-ray light curve and spectrum are reported in the *Swift* archive (http://www.swift.ac.uk/xrt_spectra/ and http://www.swift.ac.uk/xrt_curves). We have downloaded from the Swift archive and analysed the UVOT data, which cover the first 2 weeks after the explosion. The X-ray spectrum is described by a single power law with spectral index $\beta_X = 0.86 \pm 0.06$ ($F_\nu \propto \nu^{-\beta_X}$); the X-ray temporal decay, reported in Supplementary Figure 2, is well described by a double power law with a time break at $\sim$12 rest-frame days.

Under the assumption that the multi-wavelength afterglow is produced by a homogeneous jet impacting the surrounding medium and develops according to standard fireball theory, a break at a similar time should be present also in the optical light curve as required by homogeneous jet geometry and dynamics. However, the emerging of the SN light may make this difficult to observe (see Supplementary Figure 2). Following [35], we determine a jet opening angle of 40 degrees assuming a medium density of 1 cm^{-3} and the observed isotropic energy of 1.6×10^{50} erg [13].

We have constructed optical-to-X-ray spectral energy distributions at 0.62 and 2 days (corresponding to the first epoch at which $BVRI$ photometry was reported

and to the epoch of our first VLT spectrum) and reported them in Supplementary Figure 4. These show that the optical broad-band spectrum has a significantly flatter slope than the X-ray spectrum and suggests that a cooling frequency, ν_c [54] is between the optical and X-ray bands at these two epochs, and probably in the UV range covered by UVOT. If the X-rays are produced by synchrotron radiation this implies that the electron energy distribution must have a slope $p = 2 \times \beta_X = 1.72$, from which we derive in turn a synchrotron optical spectral index $\beta_{\rm opt} = (p-1)/2 = 0.36$, in agreement with the measured one, $F_{\rm opt} \propto \nu^{-0.4\pm0.1}$.

The flat electron energy distribution ($p < 2$) partially explains the shallow temporal decay of the optical and X-ray light curve before the jet break. However, we find that the standard impulsive blast wave model still predicts steeper decay if we take into account that most electron energy is carried by high energy electrons for $p < 2$ [36]. The shallow decay is likely due to a continuous energy injection from the central engine to the blast wave $L \propto t^{-q}$ [37]. The expected decay indices are consistent with the observed ones for $q = 0.84$. The expected decay index before the jet break is $\alpha = [(2+q)p + 18q - 12]/16 \sim 0.50$ below the cooling frequency (i.e. the optical band), and $[(2+q)p + 14q - 4]/16 \sim 0.79$ above the cooling frequency (i.e. the X-ray band). The index after the jet break is $\alpha = (p+6)/4 \sim 1.93$ for both below and above the cooling frequency. Since $q < 1$, the blast wave energy increases in time and it reduces the decay rates. In our light-curve decomposition we modelled the supernova with a template based on SN 1998bw, with a 10% compression in time and a dimming of 0.15 mag in the B and R bands, as observed in the spectra.

The decompositions in $BVRI$ are shown in Supplementary Figure 2. By subtracting from the light curves the constant host-galaxy flux, the afterglow component as derived from our multi-band fit, and the supernova template, we obtained the $BVRI$ light curves of SN 2016jca. These were used to construct a bolometric light curve in the range 3000–10,000 Å, which is reported in Figure 2.

We stress that in our decomposition we only used SN1998bw as a guideline to reproduce the observed points. The SN residuals are in fact rather univocally determined by host galaxy level and the afterglow model. The parameters of the latter, thanks to availability of information in many bands (X-ray, UV and optical), are rather accurately constrained (the uncertainty is $\sim$10-15% on normalization and temporal break, and less than 0.1 in time and spectral power-law indices).

The amount of ^{56}Ni synthesised in the SN presented from Figure 2, was taken from [1, 14, 5, 6].

We used the initial X-shooter spectrum to extract the fluxes of the major emission lines detected at the transient location (H_α,H_β, [OIII]$\lambda\lambda$4959,5007, and [OII]λ3727, as well as a marginal detection of [NII]λ6583). We then used the Monte Carlo code of [39] to calculate the equivalent gas-phase oxygen abundances at this location using a range of diagnostics. All of the diagnostics con-

verged to best-fit values (expressed as 12+log[O/H]) between 8.2 and 8.45, corresponding to a metallicity in the range of $0.3 < Z/Z_{\odot} < 0.55$ assuming the solar abundance of [40]. This is characteristic of other low-redshift gamma-ray burst host galaxies [20]

We use a 1D Monte Carlo radiative transfer code, which follows the propagation of photon packets through a SN atmosphere, to produce synthetic spectra. The code is based on [18, 41, 42]. This technique utilises the fact that as time passes, progressively deeper layers of the SN ejecta can be seen, since a SN can be assumed to be in homologous expansion starting $\sim 10\,\mathrm{s}$ after explosion. We have $r = v_{\mathrm{ph}} t_{\mathrm{exp}}$, where r is the distance form the centre of the explosion, v_{ph} is the photospheric velocity, and t_{exp} is the time from explosion. The Schuster-Schwarzschild approximation is used, which assumes that the radiative energy is emitted at an inner boundary in the form of a black body. This is a sound approximation for modelling a GRB-SN, as it yields good results, due to the amount of material above the photosphere. Furthermore, the approximation does not require in-depth knowledge about the radiation transport below the photosphere.
The photon packets have two fates: they either escape the ejecta or re-enter the photosphere, in a process known as back scattering. The photon packets can undergo Thomson scattering and line absorption in the ejecta. If a packet is absorbed, the downward transition it follows is determined by a photon branching scheme, which allows florescence (blue to red) and reverse florescence (red to blue) to take place. The code utilises a modified nebular approximation to treat the excitation/ionization state of the gas, to account for the non-local thermodynamical equilibrium effects caused by the diluted radiation field. There is an iteration between the radiation field and the state of the gas until convergence is achieved. Finally, the formal integral of the radiation field is computed to obtain the spectrum.
The purpose of the code is to produce optimally fitting synthetic spectra. This is done by varying input parameters, such as the bolometric luminosity, v_{ph}, and abundances. The code requires an input density profile, which can be scaled at the appropriate time from explosion for each modelled spectra, owing to the homologous expansion of the SN. We have used a modified Co381 density profile which has a $E_k = 5.4 \times 10^{52}$ erg and an ejecta mass of 8 $M_{\odot}$. This density profile was found to produce good results for SN 2003dh, which is very similar to this SN. Supplementary Table 4 contains the basic input parameters for the spectral models produced for this paper. The quality of the fits of the models to the spectra are good at all epochs, with the exception of the model at $t = 3.73\,\mathrm{d}$. This model has some success; for example, fitting the flux in the blue is very good. However the fit in the red is poor, as the afterglow contributes to most of the flux in the observations at this epoch.

Data Availability

The reduced spectra have been made available on WiseRep.

Acknowledgements

Work in this paper was based on observations made with ESO Telescopes at the Paranal Observatory under programmes ID 098.D-0055(A), 098.D-0218(A) and 298.D-5022(A).

The Liverpool Telescope is operated on the island of La Palma by Liverpool John Moores University in the Spanish Observatorio del Roque de los Muchachos of the Instituto de Astrofisica de Canarias with financial support from the UK Science and Technology Facilities Council.

Based on observations made with the TNG, operated on the island of La Palma by the Fundación Galileo Galilei of the Instituto Nazionale di Astrofisica (INAF) at the Spanish Observatorio del Roque de los Muchachos of the Instituto de Astrofsica de Canarias under programme $A32TAC_5$.

Some of the data presented herein were obtained at the W. M. Keck Observatory, which is operated as a scientific partnership among the California Institute of Technology, the University of California, and NASA; the observatory was made possible by the generous financial support of the W. M. Keck Foundation.

IRAF is the Image Reduction and Analysis Facility made available to the astronomical community by the National Optical Astronomy Observatories, which are operated by AURA, Inc., under contract with the US National Science Foundation. It is available at http://iraf.noao.edu. The work of A.V.F. has been supported by the Christopher R. Redlich Fund and the TABASGO Foundation.

SRO acknowledges the support of the Leverhulme Trust; E.Pian acknowledges Scuola Normale Superiore and INAF for support. We thank the Paranal Director for allocating Discretionary Time to this programme and the Paranal Science Operations team for their assistance; T.Krühler for assistance with X-Shooter data reduction.

A.M. acknowledges support from the ASI INAF grant I/004/11/1

Author contributions. C.A. wrote the paper and contributed the spectral models. E.Pian acquired the VLT FORS2 data, and contributed the afterglow subtraction and the bolometric light curve. P.Mazzali contributed the spectral modelling code, SN properties discussion and work coordination. E.Palazzi and F.B. reduced the VLT FORS2 spectra. S.P. and A.R. reduced the VLT FORS2, LT and Keck photometry. S.K. contributed theoretical expertise on GRB afterglows and modelling. A.L., N.R.T. and A.S.F. provided the *HST* data and image. D.P. contributed to data reduction and analysed the host galaxy metallicity. A.V.F. and

W.Z. contributed the Keck photometry. J.P.U.F. and J.S. contributed the X-Shooter spectrum for the host galaxy analysis. A.M. and P.D.A. contributed the TNG photometry. S.R.O., M.D.P., S.E. reduced and analysed the Swift/UVOT data. D.M. and P.Moller assisted with preparation and acquisition of VLT observations. G.C, K.H, K.N., M.T., A.J.C.T. and A.F.V. participated to proposals preparation and science discussion.

Bibliography

[1] Galama, T. J., Vreeswijk, P. M., van Paradijs, J., et al. 1998, Nat, 395, 670

[2] Iwamoto, K., Mazzali, P. A., Nomoto, K., et al. 1998, Nat, 395, 672

[3] Mazzali, P. A., Deng, J., Maeda, K., et al. 2002, ApJ, 572, L61

[4] Hjorth, J., Sollerman, J., Møller, P., et al. 2003, Nat, 423, 847

[5] Malesani, D., Tagliaferri, G., Chincarini, G., et al. 2004, ApJ, 609, L5

[6] D'Elia, V., Pian, E., Melandri, A., et al. 2015, A&A, 577, A116

[7] Prentice, S. J., Mazzali, P. A., Pian, E., et al. 2016, MNRAS, 458, 2973

[8] Mazzali, P. A., Deng, J., Tominaga, N., et al. 2003, ApJ, 599, L95

[9] Mazzali, P. A., Walker, E. S., Pian, E., et al. 2013, MNRAS, 432, 246

[10] Tanvir, N.R., et al. 2016, GCN 20321

[11] Pian, E. 2016, SN2016jca, TNS 2016jca

[12] Prentice, S. J., Mazzali, P. A., 2017, in prep.

[13] Fredericks, D., Golenetskii, S., Aptekar, R., et al. 2017, GCN 20323

[14] Deng, J., Tominaga, N., Mazzali, P. A., Maeda, K., & Nomoto, K. 2005, ApJ, 624, 898

[15] Richmond, M. W., van Dyk, S. D., Ho, W., et al. 1996, AJ, 111, 327

[16] Pian, E., Mazzali, P. A., Masetti, N., et al. 2006, Nat, 442, 1011

[17] Mazzali, P. A., Kawabata, K. S., Maeda, K., et al. 2005, Science, 308, 1284

[18] Mazzali, P. A. 2000, A&A, 363, 705

[19] Mazzali, P. A., Nomoto, K., Patat, F., & Maeda, K. 2001, ApJ, 559, 1047

[20] Graham, J. F., & Fruchter, A. S. 2013, ApJ, 774, 119

[21] Perley, D. A., Quimby, R. M., Yan, L., et al. 2016, ApJ, 830, 13

[22] Vergani, S. D., Salvaterra, R., Japelj, J., et al. 2015, A&A, 581, A102

[23] Krühler, T., Malesani, D., Fynbo, J. P. U., et al. 2015, A&A, 581, A125

[24] Mazzali, P. A., McFadyen, A. I., Woosley, S. E., Pian, E., & Tanaka, M. 2014, MNRAS, 443, 67

[25] Zhang, B., & Mészáros, P. 2001, ApJ, 552, L35

[26] Mazzali, P. A., Deng, J., Nomoto, K., et al. 2006, Nat, 442, 1018

[27] De Pasquale, M., Oates, S. R., Racusin, J. L., et al. 2016, MNRAS, 455, 1027

[28] MacFadyen, A. I., & Woosley, S. E. 1999, ApJ, 524, 262

[29] Woosley, S. E., & Bloom, J. S. 2006, ARA&A, 44, 507

[30] Melandri, A., Virgili, F. J., Guidorzi, C., et al. 2014, A&A, 567, A29

[31] Horne, K. 1986, PASP, 98, 609

[32] Kinney, A. L., Calzetti, D., Bohlin, R. C., et al. 1996, ApJ, 467, 38

[33] Schlafly, E. F., & Finkbeiner, D. P. 2011, ApJ, 737, 103

[34] Cardelli, J. A., Clayton, G. C., & Mathis, J. S. 1989, ApJ, 345, 245

[35] Sari, R., Piran, T., & Halpern, J. P. 1999, ApJ, 519, L17

[36] Dai, Z. G., & Cheng, K. S. 2001, ApJ, 558, L109

[37] Zhang, B., & Mészáros, P. 2004, International Journal of Modern Physics A, 19, 2385

[38] Stritzinger, M., & Leibundgut, B. 2005, A&A, 431, 423

[39] Bianco, F. B., Modjaz, M., Oh, S. M., et al. 2016, Astronomy and Computing, 16, 54

[40] Asplund, M., Grevesse, N., Sauval, A. J., & Scott, P. 2009, ARA&A, 47, 481

[41] Mazzali, P. A., & Lucy, L. B. 1993, A&A, 279, 447

[42] Lucy, L. B. 1999, A&A, 345, 211

[43] Fukugita, M., Shimasaku, K., & Ichikawa, T. 1995, PASP, 107, 945

[44] Sari, R., & Mészáros, P. 2000, ApJ, 535, L33

[45] Zhang, B., Fan, Y. Z., Dyks, J., et al. 2006, ApJ, 642, 354

[46] Maeda, K., Mazzali, P. A., & Nomoto, K. 2006, ApJ, 645, 1331

[47] C. Guidorzi, S. Kobayashi, I.A. Steele, GNC20300

[50] A. Martin-Carrillo, D. Murphy, L. Hanlon, GNC20305

[49] C. Guidorzi, S. Kobayashi, I.A. Steele, GNC20300

[50] T. Kruehler, P. Wiseman and J. Greiner, GNC20299

[51] T.Fujiwara, Y.Saito, Y. Tachibana, GNC20314

[52] Razzaque, Buckley, Hamanowicz, GNC20322

[53] N. R. Tanvir, T. Kruehler, K. Wiersema, GNC20321

[54] Sari, R., Piran, T., & Narayan, R. 1998, ApJ, 497, L17

[1]Astrophysics Research Institute, Liverpool John Moores University, IC2, Liverpool Science Park, 146 Brownlow Hill, Liverpool L3 5RF, UK
[2]INAF-IASF Bologna, Via P. Gobetti 101, 40129 Bologna, Italy
[3] Scuola Normale Superiore, Piazza dei Cavalieri 7, 56126 Pisa, Italy
[4]Max-Planck-Institut für Astrophysik, Karl-Schwarzschild-Str. 1, D-85748 Garching, Germany
[5] Department of Physics, University of Warwick, UK
[6] INAF, Astronomical Observatory of Catania, Italy
[7] Department of Astronomy, University of California, Berkeley, CA 94720-3411
[8] Dark Cosmology Centre, Niels Bohr Institute, University of Copenhagen, Juliane Maries Vej 30, 2100 København ø, Denmark
[9] INAF, Brera Astronomical Observatory, Italy
[10] Instituto de Astrofsica de Andaluca (IAA-CSIC), Glorieta de la Astronomia s/n, E-18008 Granada, Spain
[11] Mullard Space Science Laboratory, University College London, Holmbury St. Mary, Dorking, Surrey RH5 6NT, UK
[12] STScI, 3700 San Martin Dr., Baltimore, MD 20218, USA
[13] University of California, Berkeley, Space Sciences Laboratory, 7 Gauss Way, Berkeley, CA 94720-7450, USA
[14] European Southern Observatory, Karl-Schwarzschild-Str. 2, 85748 Garching bei München, Germany
[15] 5Kavli Institute for the Physics and Mathematics of the Universe (WPI), The University of Tokyo, Kashiwa, Chiba 277-8583, Japan
[16] National Astronomical Observatory of Japan, Mitaka, Tokyo 181-8588, Japan
[17] Department of Physics and Astronomy, University of Leicester, University Road, Leicester, LE1 7RH, UK
[18] Special Astrophysical Observatory, Nizhnij Arkhyz, Karachai-Cherkessian Republic, 369167 Russia